

Possible existence of super Chandrasekhar mass limit in the matter-curvature coupled gravity

N. Priyobarta ,^a S. K. Maurya ,^{b,1} Ksh. Newton Singh ,^c B. Mishra 

^aDepartment of Mathematics, Birla Institute of Technology and Science, Pilani, Hyderabad Campus, Jawahar Nagar, Kapra Mandal, Medchal District, Telangana-500078, India.

^bDepartment of Mathematical and Physical Sciences, College of Arts and Sciences, University of Nizwa, P.O. Box 33, Nizwa 616, Sultanate of Oman

^cDepartment of Physics & Astrophysics, University of Delhi, Delhi-110007, India.

E-mail: priyo.naoremcha@gmail.com, sunil@unizwa.edu.om,
ntnphy@gmail.com, bivu@hyderabad.bits-pilani.ac.in

Abstract. We investigate white dwarfs in the framework of $f(\mathcal{R}, \mathcal{L}_m)$ and $f(\mathcal{R}, \mathcal{L}_m, \mathcal{T})$ gravity to explore the Chandrasekhar Limit. We have considered two functional forms of $f(\mathcal{R}, \mathcal{L}_m)$ and one functional form of $f(\mathcal{R}, \mathcal{L}_m, \mathcal{T})$ gravity. Considering the matter Lagrangian $\mathcal{L}_m = p$, we calculate modified TOV equations for each of the forms. By employing the fully degenerate electron gas equation of state in the modified TOV equations, we derive the mass-radius relation for each functional form of both $f(\mathcal{R}, \mathcal{L}_m)$ and $f(\mathcal{R}, \mathcal{L}_m, \mathcal{T})$ gravity. Our models imply modifications in the Chandrasekhar mass limit that deviate significantly from the GR and the Newtonian cases. In the $f(\mathcal{R}, \mathcal{L}_m, \mathcal{T})$ gravity, the new mass limit of the white dwarf can reach upto $1.537 M_{\odot}$ while in $f(\mathcal{R}, \mathcal{L}_m)$ with the quadratic extension can goes upto $1.52 M_{\odot}$ and with exponential extension upto $2.08 M_{\odot}$. Further, we analyze the static stability criterion, the gravitational redshift, and the adiabatic indices. For the power-law form of $f(\mathcal{R}, \mathcal{L}_m)$ and the non-linear form of $f(\mathcal{R}, \mathcal{L}_m, \mathcal{T})$ gravity, significant variations are observed at higher densities ($\rho_c > 10^{10} \text{ g/cm}^3$), while substantial changes are noted at much lower central densities in the case of exponential form of $f(\mathcal{R}, \mathcal{L}_m)$ gravity. We also calculate compactness and gravitational redshift, which are much lower than those of neutron stars and black holes. Stability is also confirmed by adiabatic indices, which show that all models yield $\Gamma > 4/3$ throughout the interiors of WDs. Overall, our models provide a viable framework for the existence of super-Chandrasekhar mass limit, extending beyond the classical predictions in the Newtonian and/or GR cases.

Keywords: White Dwarfs, $f(\mathcal{R}, \mathcal{L}_m)$ gravity, $f(\mathcal{R}, \mathcal{L}_m, \mathcal{T})$ gravity, Chandrasekhar equation of states, Mass-Radius Relation, Stability Analysis.

¹Corresponding author

Contents

1	Introduction	1
2	Mathematical Formalism	3
2.1	The $f(\mathcal{R}, \mathcal{L}_m)$ gravity	3
2.2	The $f(\mathcal{R}, \mathcal{L}_m, T)$ gravity	5
2.3	Compact stellar models	5
2.3.1	Power-law Form of $f(\mathcal{R}, \mathcal{L}_m)$ gravity	6
2.3.2	Exponential Form of $f(\mathcal{R}, \mathcal{L}_m)$ gravity	6
2.3.3	Non-linear Form of $f(\mathcal{R}, \mathcal{L}_m, T)$ gravity	6
3	Hydrostatics Equilibrium Equations	7
4	Equation of State	7
5	Mass-Radius Analysis	8
6	Stability Analysis	11
6.1	Static Stability Criterion	12
6.2	Compactness and Gravitational Redshift	12
6.3	Adiabatic Index	15
7	Conclusions	17

1 Introduction

The general theory of relativity (GR) provides a fundamental theoretical framework for understanding various cosmic phenomena. Since its inception, GR has been crucial in advancing our understanding of a range of astrophysical and cosmological phenomena, including the behavior of planetary systems and the evolution of the Universe. Throughout the last centuries, this theory has been rigorously tested through both experiments and observations, demonstrating outstanding consistency with observed data in both weak- and strong-field conditions. The key validation of GR includes the precise prediction of the precession of Mercury's orbit [1], the detection of gravitational waves (GWs) resulting from the collisions of binary black holes and neutron stars via the LIGO and Virgo observatories [2, 3] and the observation of black hole's shadow by the Event Horizon Telescope [4]. These findings strongly support the predictions made by GR, relying on data primarily gathered since the early twentieth century. Nevertheless, GR encounters with challenges when addressing certain recent astronomical discoveries. Observations of distant supernovae in the late 1990s revealed that the universe is expanding at an accelerating pace [5–9], a behavior that GR cannot account for without incorporating additional concepts, such as dark energy. Furthermore, in

the field of astrophysical structures, various researchers have formulated theories to explain compact objects, such as neutron stars (NS), white dwarfs (WDs) and black holes (BHs), which are in the strong gravity regime.

One of the remarkable stellar objects—the white dwarf, which forms when a star has depleted its nuclear fuel and retains a compact core primarily composed of helium, carbon, and oxygen [10, 11]. More than 95% of all the observed stars in the Milky Way are WDs [12]. In most cases, WDs have carbon-oxygen (C-O) cores, which allow for larger masses compared to those of helium-core WDs. WDs resist gravitational collapse due to electron degeneracy pressure, a phenomenon arising from the Pauli exclusion principle in quantum mechanics that ultimately establishes a maximum stable mass. Chandrasekhar precisely predicted the maximum mass of the WDs for are non-rotating and non-magnetized as $1.4 M_{\odot}$ [13, 14]. This is the upper mass limit for WDs known as “the Chandrasekhar mass limit”. Recent research has revealed the existence of both over-luminous [15–18] and under-luminous [19–21] type Ia supernovae (SNe Ia), suggesting that the Chandrasekhar limit may not be universally applicable. Additionally, various observations indicate that there are masses in the range of $2.1 - 2.8 M_{\odot}$, which significantly surpass the upper limit [22, 23], thereby challenging the uniqueness of the Chandrasekhar limit and the current theory of GR.

These observations, along with the cosmological problems, motivate us to modify the existing theory of GR [24, 25]. By treating the Lagrangian as an arbitrary function of the Ricci scalar \mathcal{R} , Felice and Tsujikawa [26] develop a class of $f(\mathcal{R})$ theories that serve as an alternative explanation for the accelerated expansion of the universe, without considering dark energy. On top of that, $f(\mathcal{R})$ models provide a wide variety of phenomenological implications in cosmological [27–30]. In the field of compact objects like NS, the $f(\mathcal{R})$ theories provided the very prominent results [31–36]. Ganguly et al. formulated NS with the functional form of $f(\mathcal{R}) = \mathcal{R} + \alpha\mathcal{R}^2$, which is also known as the Starobinsky model, and described how some of the EoS can match all conditions provided at the surface of the NS. [37]. Astashenok et al. provided the stable NS of maximum mass $> 2 M_{\odot}$ [38] using various relativistic EoS. Further, by considering $f(\mathcal{R}) = \mathcal{R} + \mathcal{R} [\exp(-\mathcal{R}/\mathcal{R}_0) - 1]$ and \mathcal{R}^2 models with logarithmic and cubic corrections, they have obtained $2.2 - 2.3 M_{\odot}$ [39], which explains the mass-gap of the NS-BHs in astrophysical scenarios. In the context of WDs, many researchers have also been interested in studying their mass and radius in light of modified theories [40–44]. In addition to the $f(\mathcal{R})$ theories, various modified gravity theories are formulated and analyzed WDs such as $f(\mathcal{R}, \mathcal{T})$ [45, 46], Palatini $f(\mathcal{R})$ [47, 48], Rastall-Rainbow [49] and scalar-tensor theories [50].

One way to modify the theory is by considering non-minimal matter-geometry coupling to gravity. In this theory, matter and geometry are non-minimally coupled to each other [51–53]. As a similar approach to $f(\mathcal{R})$ gravity, Harko and Lobo proposed the $f(\mathcal{R}, \mathcal{L}_m)$ gravity theory, which generalizes the action to an arbitrary function that depends on both \mathcal{R} and \mathcal{L}_m [54]. This theory can be viewed as an extensive expansion of earlier models, merging contributions from both curvature and matter into a unified functional expression. The non-minimal coupling present in $f(\mathcal{R}, \mathcal{L}_m)$ gravity indicates a covariant non-conservation of the energy-momentum tensor, resulting in the non-

geodesic motion of test particles and the emergence of an additional force. Notably, the explicit violation of the equivalence principle renders this theory amenable to direct testing through astrophysical observations and solar-system constraints [55, 56].

In the context of $f(\mathcal{R}, \mathcal{L}_m)$ gravity, researchers have examined various phenomena, particularly compact stars [57]. Lobato et al. [58] investigated the interaction between \mathcal{R} and \mathcal{L}_m , which constrain GWs and massive pulsars such as GW170817 and PSR J0030+0451. Additionally, studies of wormholes have uncovered intriguing structures within the $f(\mathcal{R}, \mathcal{L}_m)$ gravity framework, yielding positive results [59–61]. Recent research has also looked into energy conditions [62] and the cosmological effects [63–65] related to $f(\mathcal{R}, \mathcal{L}_m)$ gravity. Lobato et al. [57] considered $f(\mathcal{R}, \mathcal{L}_m) = \mathcal{R}/2 + \mathcal{L}_m + \sigma \mathcal{R} \mathcal{L}_m$ predicted the maximum masses which are above the Chandrasekhar mass limit.

Furthermore, building upon the concepts of unification of $f(\mathcal{R}, \mathcal{L}_m)$ [54] and $f(\mathcal{R}, \mathcal{T})$ [66] gravity, Haghani and Harko developed these theories into a more generalized coupling between geometry and matter, referred to as $f(\mathcal{R}, \mathcal{L}_m, \mathcal{T})$ gravity [67]. In this theory, Haghani and Harko examine the Lagrangian as an arbitrary function of the Ricci scalar \mathcal{R} , the matter Lagrangian \mathcal{L}_m , and the trace of the energy-momentum tensor \mathcal{T} . Further, one can still reduce $f(\mathcal{R}, \mathcal{L}_m, \mathcal{T})$ gravity to $f(\mathcal{R})$, $f(\mathcal{R}, \mathcal{L}_m)$ and $f(\mathcal{R}, \mathcal{T})$ gravity as provided in Ref. [68]. Recently, extensive research has explored various aspects of $f(\mathcal{R}, \mathcal{L}_m, \mathcal{T})$ gravity, such as wormholes [69], compact objects [68, 70], and in the context of cosmological implications [71]. In the context of $f(\mathcal{R}, \mathcal{L}_m, \mathcal{T})$, Oteniel et al. [72] provided the possibility of the existence of WDs beyond the Chandrasekhar mass limit.

In this article, we will investigate both $f(\mathcal{R}, \mathcal{L}_m)$ and $f(\mathcal{R}, \mathcal{L}_m, \mathcal{T})$ gravity. We will study their impacts on the structure of WDs, focusing on mass-radius relations and the stability of the system. For $f(\mathcal{R}, \mathcal{L}_m)$ gravity, we will consider two functional models i.e., power-law [$f(\mathcal{R}, \mathcal{L}_m) = \mathcal{R}/16\pi + \mathcal{L}_m + \sigma \mathcal{L}_m^2$] and exponential form [$f(\mathcal{R}, \mathcal{L}_m) = \mathcal{R}/16\pi + [1 - \gamma \exp(-\sqrt{\beta \mathcal{L}_m})] \mathcal{L}_m$], whereas in the case of $f(\mathcal{R}, \mathcal{L}_m, \mathcal{T})$, a non-linear functional form [$f(\mathcal{R}, \mathcal{L}_m, \mathcal{T}) = \mathcal{R} + \alpha \mathcal{L}_m \mathcal{T}$] are considered. We also analyze various stability criteria in order to ensure the physical viability of the WD models. Throughout the article, we will adopt the system of units in which $G = c = 1$.

The structure of the article: in section 2, the field equations for both $f(\mathcal{R}, \mathcal{L}_m)$ and $f(\mathcal{R}, \mathcal{L}_m, \mathcal{T})$ gravity are introduced, along with their respective models. Section 3 includes the computation of the TOV equations for each model, while section 4 offers a brief summary of Chandrasekhar’s equation of state for degenerate WDs. The numerical analysis and the mass-radius analysis are presented in section 5. Various stability analyses are conducted in section 6. Finally, section 7 presents the conclusions.

2 Mathematical Formalism

2.1 The $f(\mathcal{R}, \mathcal{L}_m)$ gravity

The theory provides the gravitational Lagrangian as a function of Ricci scalar \mathcal{R} and matter Lagrangian \mathcal{L}_m . In this framework, the action of $f(\mathcal{R}, \mathcal{L}_m)$ gravity [54] is given

as,

$$S = \int f(\mathcal{R}, \mathcal{L}_m) \sqrt{-g} d^4x, \quad (2.1)$$

where $f(\mathcal{R}, \mathcal{L}_m)$ be an arbitrary function of \mathcal{R} and \mathcal{L}_m , respectively denote the Ricci scalar and matter Lagrangian. Assuming the matter Lagrangian only depends on the metric [73], we defined the energy-momentum tensor of the matter as

$$\mathcal{T}_{\mu\nu} = g_{\mu\nu} \mathcal{L}_m - 2 \frac{\partial \mathcal{L}_m}{\partial g^{\mu\nu}}. \quad (2.2)$$

By varying the action (2.1), the field equations of $f(\mathcal{R}, \mathcal{L}_m)$ gravity can be obtained as

$$\begin{aligned} f_{\mathcal{R}}(\mathcal{R}, \mathcal{L}_m) \mathcal{G}_{\mu\nu} + \frac{1}{2} g_{\mu\nu} \left[f_{\mathcal{R}}(\mathcal{R}, \mathcal{L}_m) \mathcal{R} - f(\mathcal{R}, \mathcal{L}_m) + f_{\mathcal{L}}(\mathcal{R}, \mathcal{L}_m) \mathcal{L}_m \right] \\ = \frac{1}{2} f_{\mathcal{L}}(\mathcal{R}, \mathcal{L}_m) \mathcal{T}_{\mu\nu} - \left(g_{\mu\nu} \square - \nabla_{\mu} \nabla_{\nu} \right) f_{\mathcal{R}}(\mathcal{R}, \mathcal{L}_m). \end{aligned} \quad (2.3)$$

For brevity, we denote

$$f_{\mathcal{R}}(\mathcal{R}, \mathcal{L}_m) = \frac{\partial f(\mathcal{R}, \mathcal{L}_m)}{\partial \mathcal{R}} \quad \text{and} \quad f_{\mathcal{L}}(\mathcal{R}, \mathcal{L}_m) = \frac{\partial f(\mathcal{R}, \mathcal{L}_m)}{\partial \mathcal{L}_m}.$$

On substituting $f(\mathcal{R}, \mathcal{L}_m) = \mathcal{R}/2 + \mathcal{L}_m$ in Eq. (2.3), one can retrieve the standard field equations of GR. The divergence of the energy-momentum tensor $\mathcal{T}_{\mu\nu}$ can be given as,

$$\nabla^{\mu} \mathcal{T}_{\mu\nu} = \nabla^{\mu} \ln \left[f_{\mathcal{L}}(\mathcal{R}, \mathcal{L}_m) \right] (\mathcal{L}_m g_{\mu\nu} - \mathcal{T}_{\mu\nu}). \quad (2.4)$$

In this article, we have proposed two functional forms of $f(\mathcal{R}, \mathcal{L}_m)$ gravity as

- Power-law form [54]:

$$f(\mathcal{R}, \mathcal{L}_m) = \frac{\mathcal{R}}{16\pi} + \mathcal{L}_m + \sigma \mathcal{L}_m^2, \quad (2.5)$$

where σ is coupling parameter and has a dimension of cm^2/dyne .

- Exponential form [54]:

$$f(\mathcal{R}, \mathcal{L}_m) = \frac{\mathcal{R}}{16\pi} + \left[1 - \gamma \exp \left(- \sqrt{\beta \mathcal{L}_m} \right) \right] \mathcal{L}_m, \quad (2.6)$$

where γ and β are coupling parameter. For simplicity, β is fixed at 2, and the values of γ are varied. The parameter β has a unit of cm^2/dyne while γ is dimensionless parameter.

2.2 The $f(\mathcal{R}, \mathcal{L}_m, \mathcal{T})$ gravity

As an extension to the $f(\mathcal{R}, \mathcal{L}_m)$ gravity, we also consider $f(\mathcal{R}, \mathcal{L}_m, \mathcal{T})$, which non minimally couples with the trace of the energy-momentum tensor, \mathcal{T} . The action for $f(\mathcal{R}, \mathcal{L}_m, \mathcal{T})$ gravity [67] can be given as,

$$S = \frac{1}{16\pi} \int f(\mathcal{R}, \mathcal{L}_m, \mathcal{T}) \sqrt{-g} d^4x + \int \mathcal{L}_m \sqrt{-g} d^4x. \quad (2.7)$$

Here, the function $f(\mathcal{R}, \mathcal{L}_m, \mathcal{T})$ is an arbitrary function of the Ricci scalar \mathcal{R} , matter Lagrangian \mathcal{L}_m and \mathcal{T} be the trace of energy momentum tensor $\mathcal{T}_{\mu\nu}$. Varying the action (2.7) with respect to the metric $g^{\mu\nu}$, the field equations of $f(\mathcal{R}, \mathcal{L}_m, \mathcal{T})$ gravity obtained as,

$$\begin{aligned} f_{\mathcal{R}} \mathcal{R}_{\mu\nu} + (g_{\mu\nu} \square - \nabla_{\mu} \nabla_{\nu}) f_{\mathcal{R}} - \frac{1}{2} \left[f - (f_{\mathcal{L}} + 2f_{\mathcal{T}}) \mathcal{L}_m \right] g_{\mu\nu} \\ = \left[8\pi + \frac{1}{2} (f_{\mathcal{L}} + 2f_{\mathcal{T}}) \right] \mathcal{T}_{\mu\nu} + \tau_{\mu\nu} f_{\mathcal{T}}. \end{aligned} \quad (2.8)$$

Here, $f = f(\mathcal{R}, \mathcal{L}_m, \mathcal{T})$, $f_{\mathcal{R}} = \partial f / \partial \mathcal{R}$, $f_{\mathcal{L}} = \partial f / \partial \mathcal{L}_m$, $f_{\mathcal{T}} = \partial f / \partial \mathcal{T}_m$, $\mathcal{R}_{\mu\nu}$ represents the Ricci tensor and ∇ be the covariant derivative with respect to the symmetric connection associated to $g_{\mu\nu}$. On substitution, $f(\mathcal{R}, \mathcal{L}_m, \mathcal{T}) = \mathcal{R}$, Eq.(2.8) can reduce to GR. The tensor, $\tau_{\mu\nu}$ can be defined as [67],

$$\tau_{\mu\nu} = 2 g^{\sigma\delta} \frac{\partial^2 \mathcal{L}_m}{\partial g^{\mu\nu} \partial g^{\sigma\delta}}. \quad (2.9)$$

Taking the covariant derivative of Eq. (2.8) and using the geometric identity only [74] $[\square, \nabla_{\nu}] f_{\mathcal{R}} = \mathcal{R}_{\mu\nu} \nabla^{\mu} f_{\mathcal{R}}$, one can obtain the non-conservative energy-momentum tensor as,

$$\nabla^{\mu} \mathcal{T}_{\mu\nu} = \frac{1}{8\pi + f_m} \left[\nabla_{\nu} (\mathcal{L}_m f_m) - \mathcal{T}_{\mu\nu} \nabla^{\mu} f_m - \mathcal{A}_{\nu} - \frac{1}{2} \left(f_{\mathcal{T}} \nabla_{\nu} \mathcal{T} + f_{\mathcal{L}} \nabla_{\nu} \mathcal{L}_m \right) \right], \quad (2.10)$$

where $f_m = f_{\mathcal{T}} + \frac{1}{2} f_{\mathcal{L}}$ and $\mathcal{A}_{\nu} = \nabla^{\mu} (f_{\mathcal{T}} \tau_{\mu\nu})$. In case of $f(\mathcal{R}, \mathcal{L}_m, \mathcal{T})$ will be consider only the non-linear or multiplicative case [67]:

$$f(\mathcal{R}, \mathcal{L}_m, \mathcal{T}) = \mathcal{R} + \alpha \mathcal{L}_m \mathcal{T}, \quad (2.11)$$

where α is the coupling parameter with the units of cm^2/dyne .

2.3 Compact stellar models

Throughout the paper, we consider the static spherically symmetric $4 - D$ spacetime as given by the metric,

$$ds^2 = -e^{\xi(r)} dt^2 + e^{\lambda(r)} dr^2 + r^2 d\theta^2 + r^2 \sin^2 \theta d\phi^2, \quad (2.12)$$

where $\xi(r)$ and $\lambda(r)$ are functions of r only. The interior of the star is an isotropic and perfect fluid, given as

$$\mathcal{T}_{\mu\nu} = (\rho + p) u_{\mu} u_{\nu} + p g_{\mu\nu}, \quad (2.13)$$

where $\rho(r)$ and $p(r)$ are the energy density and pressure of matter, respectively. $u_{\mu} = \{e^{\xi/2}, 0, 0, 0\}$ denotes the four velocity of the fluid. We also consider the matter Lagrangian, $\mathcal{L}_m = p$, in all the cases.

2.3.1 Power-law Form of $f(\mathcal{R}, \mathcal{L}_m)$ gravity

For the power-law choice of $f(\mathcal{R}, \mathcal{L}_m)$ gravity (2.5), the field equation (2.3) becomes

$$\mathcal{G}_{\mu\nu} = 8\pi \left[(1 + 2\sigma \mathcal{L}_m) \mathcal{T}_{\mu\nu} - \sigma g_{\mu\nu} \mathcal{L}_m^2 \right], \quad (2.14)$$

where the tt and rr components respectively become,

$$e^{-\lambda} \left(\frac{\lambda'}{r} - \frac{1}{r^2} \right) + \frac{1}{r^2} = 8\pi\sigma p^2 + 8\pi(1 + 2\sigma p)\rho, \quad (2.15)$$

$$e^{-\lambda} \left(\frac{\xi'}{r} + \frac{1}{r^2} \right) - \frac{1}{r^2} = 8\pi(p + \sigma p^2). \quad (2.16)$$

From the covariant derivative of energy-momentum tensor (2.4), we get

$$\frac{dp}{dr} = -(\rho + p) \frac{\xi'}{2}. \quad (2.17)$$

2.3.2 Exponential Form of $f(\mathcal{R}, \mathcal{L}_m)$ gravity

For the exponential-form of $f(\mathcal{R}, \mathcal{L}_m)$ gravity (2.6), the field equation (2.3) becomes

$$\mathcal{G}_{\mu\nu} = 8\pi \left[\frac{1}{2} \gamma e^{-\sqrt{\beta p}} \left(\sqrt{\beta p} - 2 \right) + 1 \right] \mathcal{T}_{\mu\nu} - 4\pi g_{\mu\nu} \left[\gamma p e^{-\sqrt{\beta p}} \sqrt{\beta p} \right], \quad (2.18)$$

with tt and rr components are respectively,

$$\sqrt{\beta p} \left[e^{\sqrt{\beta p}} (r\lambda' + e^\lambda - 1) - 8\pi r^2 e^\lambda \rho (e^{\sqrt{\beta p}} - \gamma) \right] = 4\pi\gamma\beta r^2 p e^\lambda \rho + 4\pi\gamma\beta r^2 p^2 e^\lambda, \quad (2.19)$$

$$e^\lambda - r\xi' - 1 = 8\pi r^2 p e^\lambda \left(\gamma e^{-\sqrt{\beta p}} - 1 \right). \quad (2.20)$$

Also, from Eq. (2.4) we obtained

$$\frac{dp}{dr} = -(\rho + p) \frac{\xi'}{2}. \quad (2.21)$$

2.3.3 Non-linear Form of $f(\mathcal{R}, \mathcal{L}_m, \mathcal{T})$ gravity

With the non-linear model (2.11), the field equation (2.8) reduces to

$$G_{\mu\nu} = \left[8\pi + \frac{\alpha}{2}(5p - \rho) \right] \mathcal{T}_{\mu\nu} + \alpha p^2 g_{\mu\nu}. \quad (2.22)$$

The tt and rr components are obtained respectively as,

$$e^{-\lambda} \left(\frac{\lambda'}{r} - \frac{1}{r^2} \right) + \frac{1}{r^2} = \frac{1}{2} \left[5\alpha p \rho + 2\alpha p^2 + \rho(16\pi - \alpha\rho) \right], \quad (2.23)$$

$$e^{-\lambda} \left(\frac{\xi'}{r} + \frac{1}{r^2} \right) - \frac{1}{r^2} = \frac{1}{2} \left[16\pi + 3\alpha p - \alpha\rho \right] p. \quad (2.24)$$

Also, from the covariant derivative of energy-momentum tensor (2.10), we obtain

$$p' + (\rho + p) \frac{\xi'}{2} = \frac{\alpha p (\rho' - p')}{16\pi + \alpha(5p - \rho)}, \quad (2.25)$$

where prime denotes the derivative with respect to the radial coordinate.

3 Hydrostatics Equilibrium Equations

For all cases, the boundary condition of the metric potential $e^{-\lambda}$ is considered as the Schwarzschild exterior solution given as,

$$e^{-\lambda} = 1 - \frac{2m(r)}{r}, \quad (3.1)$$

where $m(r)$ is the gravitational mass.

For the power-law form, using the Schwarzschild exterior solution with Eq. (2.16)–Eq. (2.17), the modified TOV-equations can be provided as

$$\frac{dm}{dr} = 8\pi r^2 \left[\rho + \sigma p(p + 2\rho) \right], \quad (3.2)$$

$$\frac{dp}{dr} = -\frac{(p + \rho) [m + 4\pi r^3 p(1 + \sigma p)]}{r^2 (1 - 2m/r)}. \quad (3.3)$$

For the exponential form, using the Schwarzschild exterior solution with (2.20)–(2.21), the modified TOV equations are reduced to

$$\frac{dm}{dr} = 4\pi r^2 \rho + \left[2\pi \gamma r^2 \rho \sqrt{\beta p} - 4\pi \gamma r^2 \rho + 2\pi \gamma r^2 p \sqrt{\beta p} \right] e^{-\sqrt{\beta p}}, \quad (3.4)$$

$$\frac{dp}{dr} = -\frac{(p + \rho) \left[(m + 4\pi r^3 p) - 4\pi \gamma r^3 p e^{-\sqrt{\beta p}} \right]}{r^2 (1 - 2m/r)}. \quad (3.5)$$

Using boundary condition and (2.23)–(2.25), the modified TOV equations of non-linear form of $f(\mathcal{R}, \mathcal{L}_m, \mathcal{T})$ gravity become,

$$\frac{dm}{dr} = 4\pi r^2 \rho + \frac{\alpha r^2}{4} \left[2p^2 + \rho(5p - \rho) \right], \quad (3.6)$$

$$\frac{dp}{dr} = -\frac{(p + \rho) (16\pi + 5\alpha p - \alpha\rho) [4m + pr^3 (16\pi + 3\alpha p - \alpha\rho)]}{4r^2 (1 - 2m/r) (16\pi - \alpha [(dp/dp - 6)p + \rho])}. \quad (3.7)$$

To calculate the modified TOV equations for each case, we must consider EoS of fully degenerate electron gas, which we will discuss in the next section.

4 Equation of State

To solve differential equation systems for each case such as, (3.2)–(3.3), (3.4)–(3.5) and (3.6)–(3.7), we need to consider an appropriate EoS that provides $p(\rho)$. For WDs, we considered Chandrasekhar EoS at zero temperature describing a completely degenerate relativistic gas [14]. For a completely degenerate e^- gas, the number of electrons N in a finite volume V in an arbitrary momentum P and below the Fermi momentum P_F are respectively given as

$$N = V \frac{8\pi P^3}{h^3}, \quad N = V \frac{8\pi}{h^3} \int_0^{P_F} P^2 dP = V \frac{8\pi}{3h^3} P_F^3. \quad (4.1)$$

The pressure generated by the e^- gas can be calculated as

$$p = \frac{1}{3V} \int_0^\infty N(P) P v_P dP = \frac{1}{3V} \int_0^{P_F} N(P) P v_P dP = \frac{1}{3V} \int_0^{P_F} N(P) P \frac{\partial E}{\partial P} dP, \quad (4.2)$$

where v_P and E are the velocity and kinetic energy corresponding to the momentum P . For relativistic electrons, the kinetic energy can be written as

$$E = m_e c^2 \left[\left(1 + \frac{P^2}{m_e^2 c^2} \right)^{1/2} - 1 \right] \quad \text{or} \quad \frac{\partial E}{\partial P} = \frac{P}{m_e} \left(1 + \frac{P^2}{m_e^2 c^2} \right)^{-1/2}, \quad (4.3)$$

leading to

$$p = \frac{8\pi}{3m_e h^3} \int_0^{P_F} \frac{P^4 dP}{(1 + P^2/m_e^2 c^2)^{1/2}}, \quad (4.4)$$

which integrates by a variable transformation $\sinh \theta = P/m_e c$ as

$$p = \frac{8\pi m_e^4 c^5}{3h^3} \int_0^{\theta_F} \sinh^4 \theta d\theta = \frac{8\pi m_e^4 c^5}{3h^3} \left[\frac{\sinh^3 \theta_F \cosh \theta_F}{4} - \frac{3 \sinh(2\theta_F)}{16} + \frac{3\theta_F}{8} \right]. \quad (4.5)$$

This further reduces to

$$p(X_F) = \frac{\pi m_e^4 c^5}{3h^3} \left[(2X_F^3 - 3X_F) \sqrt{X_F^2 + 1} + 3 \sinh^{-1} X_F \right], \quad (4.6)$$

$$\rho(X_F) = n_e \mu_e m_p = \frac{8\pi \mu_e m_p (m_e c)^3}{3h^3} X_F^3, \quad (4.7)$$

where $X_F := P_F/m_e c$ is the dimensionless Fermi momentum, m_e the electron mass, m_p the proton mass, h is the usual Plank's constant and μ_e is the molecular weight per electron. For our article, we will consider C-O WDs, whose molecular weight, $\mu_e \approx 2$.

5 Mass-Radius Analysis

The results for WDs are presented using the fully degenerate EoS given in the previous section. The mass and radius of WDs are obtained by numerically solving the modified TOV-equations (3.2)–(3.7). We consider the range of central densities, ρ_c and repeatedly compute WD structures. To numerically solve these equations, we also utilize dimensionless physical variables as described in Ref. [75] and apply the boundary conditions at $r = 0$ as

$$\rho(0) = \rho_c \quad \text{and} \quad m(0) = 0, \quad (5.1)$$

where ρ_c is the central density. We compute the integration until the pressure decreases to zero at the point where $p(R) = 0$. We consider this point to be the surface of the WDs and denote its radius as R . Finally, using this radius R , we calculate the

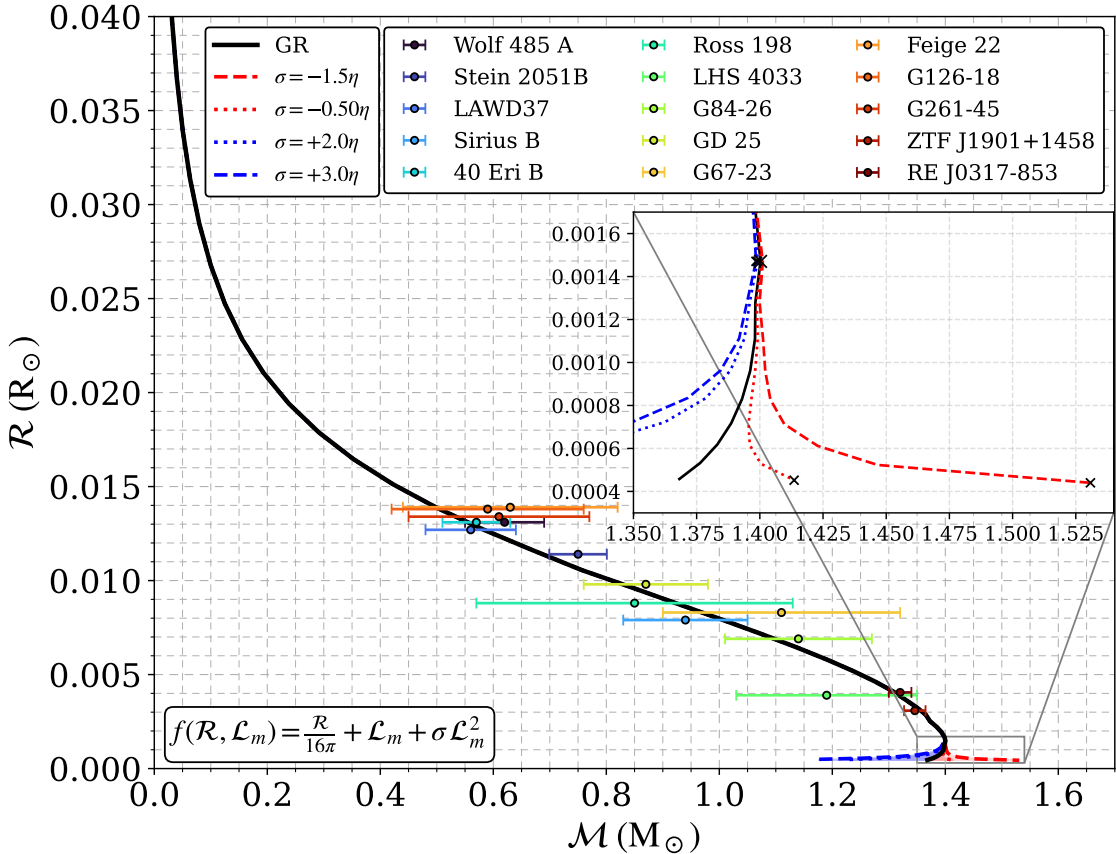


Figure 1: $M - R$ plot for WDs within $f(\mathcal{R}, \mathcal{L}_m)$ gravity power-law form. The solid black curve represents the predictions of GR, while the colored curves depict various values of the coupling parameter σ , which range from -1.50η to $+3.0\eta$, with η approximately equal to $1.8 \times 10^{-32} \text{ cm}^2/\text{dyne}$.

maximum mass of the WDs. We have also converted all the coupling parameters to dimensionless quantities. By repeatedly calculating the structure of WDs over the range of central density $1 \times 10^7 - 2.4 \times 10^{12} \text{ g/cm}^3$, we obtain the mass-radius relation for each of the model of both $f(\mathcal{R}, \mathcal{L}_m)$ and $f(\mathcal{R}, \mathcal{L}_m, \mathcal{T})$ gravity. We also included some observational constraints for well-known WDs from the catalogue of Ref [76].

In the power-law model of $f(\mathcal{R}, \mathcal{L}_m)$ gravity, we examined values of σ ranging from -1.5η to $+3.0\eta$, as illustrated in Figure 1. The effects of the $\sigma \mathcal{L}_m^2$ term are particularly noticeable at high densities, specifically for densities $\rho_c \geq 10^{10} \text{ g/cm}^3$. Notably, with negative values of σ , it is possible to achieve a higher mass compared to the GR and/or Newtonian scenario. For $\sigma = -1.5\eta$ and $\sigma = -0.50\eta$, the model can generate maximum masses of up to $1.52M_\odot$ and $1.41M_\odot$, respectively. Further, we also provided the maximum mass and radii in units of solar mass and solar radii for the different values of σ in Table 1.

In the case of the exponential model of $f(\mathcal{R}, \mathcal{L}_m)$ gravity, we consider the value of

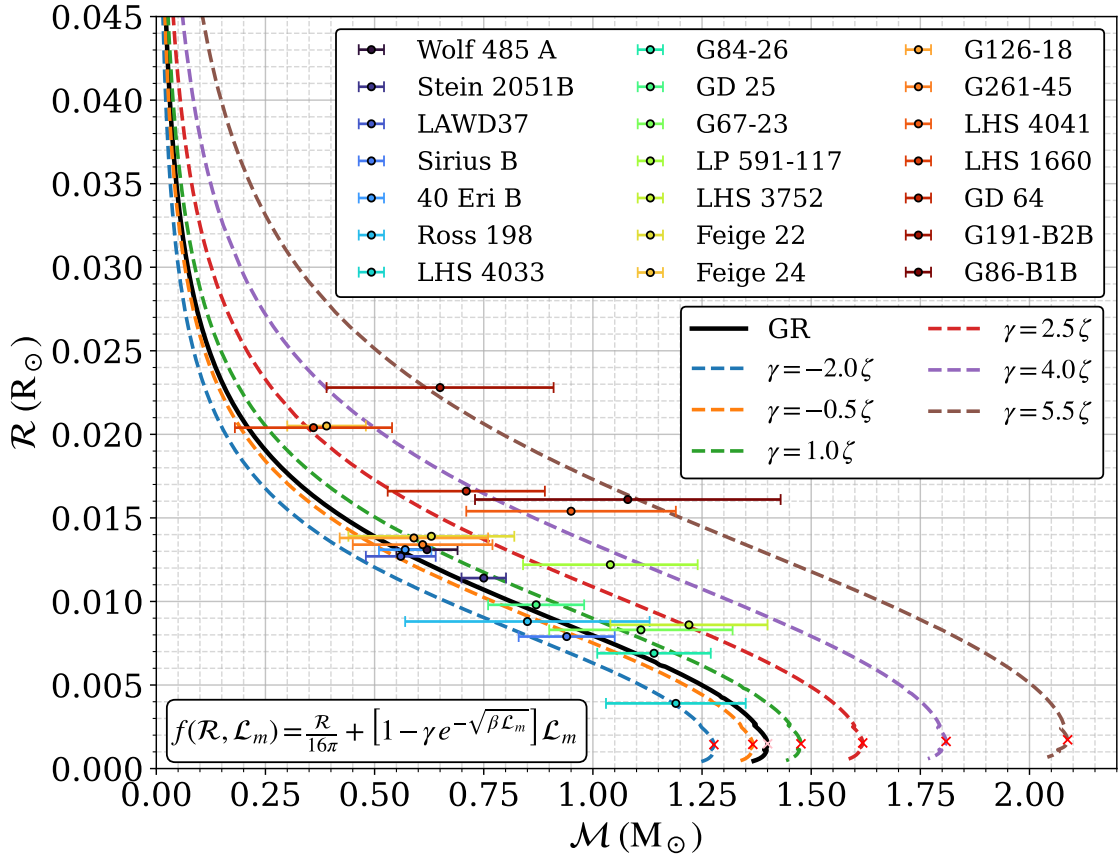


Figure 2: $M - R$ diagram for WDs in the $f(\mathcal{R}, \mathcal{L}_m)$ gravity with an exponential form. For simplification purposes, we set the value of $\beta = 2$ with units of $\text{cm}^2 \text{dyne}^{-1}$ while considering values of γ from -2.0ζ to 5.5ζ . The solid black line represents the predictions from GR, while the dashed lines represent various values of the coupling parameter γ , measured in dimensionless units with the value of $\zeta = 10^{-1}$.

$\beta = 2$ and vary the value of γ as shown in the Figure 2. We have considered both positive and negative values, ranging from -2.0ζ to 5.5ζ , along with GR. The effects of the exponential terms are clearly evident in the model, where positive values of γ can result in higher mass. With the values of $\gamma = 5.5\zeta$, one can generate maximum mass up $2.08M_\odot$, which is higher than the maximum mass of GR and Newtonian cases. We also provided the maximum mass and radii of each value of γ in Table 2.

Finally, for the non-linear model of $f(\mathcal{R}, \mathcal{L}_m, \mathcal{T})$ gravity, we have plotted $M - R$ curve, as shown in Figure 3. By varying the values of α with the ranges from -3.0χ to $+5.0\chi$, we examined how the $M - R$ curve changes and effects of the coupling term is particularly noticeable at high densities, specifically for densities $\rho_c \geq 10^{10} \text{g/cm}^3$. as similar to the power-law model of $f(\mathcal{R}, \mathcal{L}_m)$ gravity. Otoniel et al. [72] also provided similar plots in the non-linear form of $f(\mathcal{R}, \mathcal{L}_m, \mathcal{T})$ gravity. In this case, maximum mass can be generated with the negative values of α . With the value of $\alpha = +5.0\chi$,

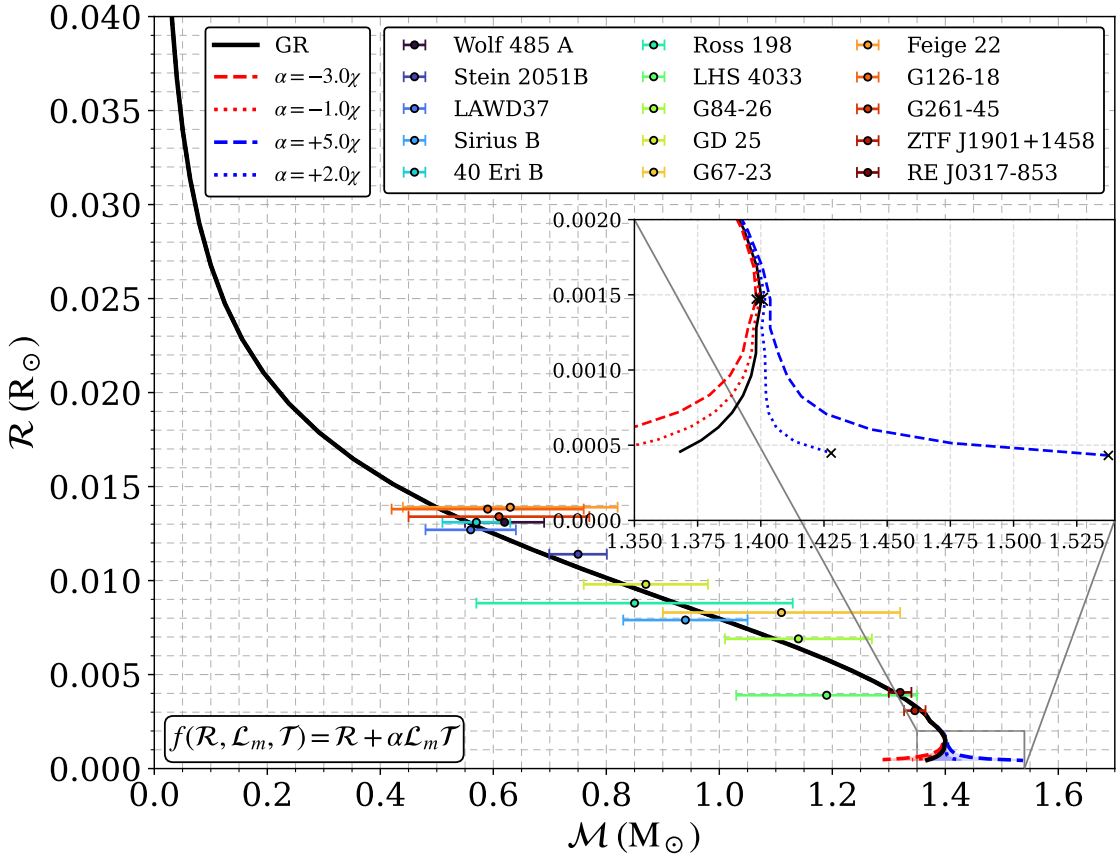


Figure 3: $M - R$ plot for WDs within the non-linear model of $f(\mathcal{R}, \mathcal{L}_m, \mathcal{T})$ gravity. The solid black curve represents the predictions of GR, while the colored curves depict various values of the coupling parameter α , which range from -3.0χ to $+2.0\chi$, with χ approximately equal to $1.6 \times 10^{-12} \text{ cm}^3/\text{g}$.

one can generate the maximum mass of $1.53M_\odot$. Table 3 provides the maximum mass and corresponding radii for each value of the parameter.

In all the models examined, it is evident that the mass can be significantly higher than the GR and the Newtonian predictions. Additionally, the observational masses of WDs can provide important constraints. Higher-mass WDs, such as ZTF J1901+1458 [77] and RE J0317-853 [78], play a crucial role in constraining these models. Furthermore, WDs described by the exponential model of $f(\mathcal{R}, \mathcal{L}_m)$ gravity, such as G86-B1B, LHS 3752, GD 64, and G191-B2B, cannot be adequately constrained by the non-linear model of $f(\mathcal{R}, \mathcal{L}_m, \mathcal{T})$ gravity or the power-law model of $f(\mathcal{R}, \mathcal{L}_m)$ gravity.

6 Stability Analysis

To develop effective models, we examine different stability criteria to ensure that the systems do not collapse. Stability can be evaluated through various approaches. Here,

we have three approaches such as (i) static stability criterion, (ii) compactness and gravitational redshift, and (iii) adiabatic index.

6.1 Static Stability Criterion

We analyze the stability using the general relativistic case, $dM/d\rho_c > 0$, i.e., as the central density increases, the mass increases until it reaches the maximum mass. For the power-law model of $f(\mathcal{R}, \mathcal{L}_m)$ gravity, gravitational mass also increases monotonically with central density until it reaches maximum mass. Over the ranges of σ from -1.5η to $+3.0\eta$, we have plotted the $M - \rho_c$ curve as shown in the Figure. 4. For all the consideration of σ , the given conditions hold upto the maximum mass configuration. Positive values of σ , the central density of the maximum mass hold $\rho_c \approx 10^{10} \text{ g/cm}^3$ whereas negative values hold up to $\rho_c \approx 10^{12} \text{ g/cm}^3$.

Using the same criterion, we also analyze the exponential form of $f(\mathcal{R}, \mathcal{L}_m)$ gravity. The $M - \rho_c$ plot for GR and for the coupling parameter γ in the range of -2.0ζ to -5.5ζ are shown in Figure 4. For both GR and all considered values of γ , gravitational mass also increases monotonically with central density until it reaches maximum mass, which satisfies the condition $dM/d\rho_c > 0$. For all cases, the central density of the maximum mass lies in the range of $10^{10} < \rho_c < 10^{11} \text{ g/cm}^3$. Finally, in the non-linear model of $f(\mathcal{R}, \mathcal{L}_m, \mathcal{T})$ gravity, the gravitational mass monotonically increases with central density until it reaches its maximum mass. We have plotted the $M - \rho_c$ curve for the range of α from -3.0χ to $+5.0\chi$, as illustrated in Figure 5. For every value of α considered, the specified conditions remain valid up to the maximum mass configuration. For negative values of α , the central density at maximum mass is approximately $\rho_c \approx 10^{10} \text{ g/cm}^3$, while for positive values, it reaches about $\rho_c \approx 10^{12} \text{ g/cm}^3$. For all the models considered, the coupling parameter satisfies the stability criterion, i.e., $dM/d\rho_c > 0$. Central density as high as $\sim 10^{12} \text{ g/cm}^3$ are obtained in the case of power-law model of $f(\mathcal{R}, \mathcal{L}_m)$ gravity and non-linear model of $f(\mathcal{R}, \mathcal{L}_m, \mathcal{T})$ gravity. In contrast, the exponential model of $f(\mathcal{R}, \mathcal{L}_m)$ gravity yields lower central densities in the ranges $10^{10} - 10^{11} \text{ g/cm}^3$.

6.2 Compactness and Gravitational Redshift

The gravitational redshift enables us to measure the strength of the gravitational field around WDs, thereby deepening our understanding of gravitational behavior in extreme environments. Additionally, we examine the correlation between surface gravitational redshift Z_s and mass for WDs. The surface gravitational redshift is defined as

$$Z_s = \frac{1}{\sqrt{1 - 2C}} - 1 . \quad (6.1)$$

Here, $C = M/R$ is the compactness of the stellar structures. Due to the relatively large radii and lower masses compared to other compact objects like neutron stars, WDs have very small compactness values, leading to low surface gravitational redshifts on the order of $\mathcal{O}(10^{-3})$.

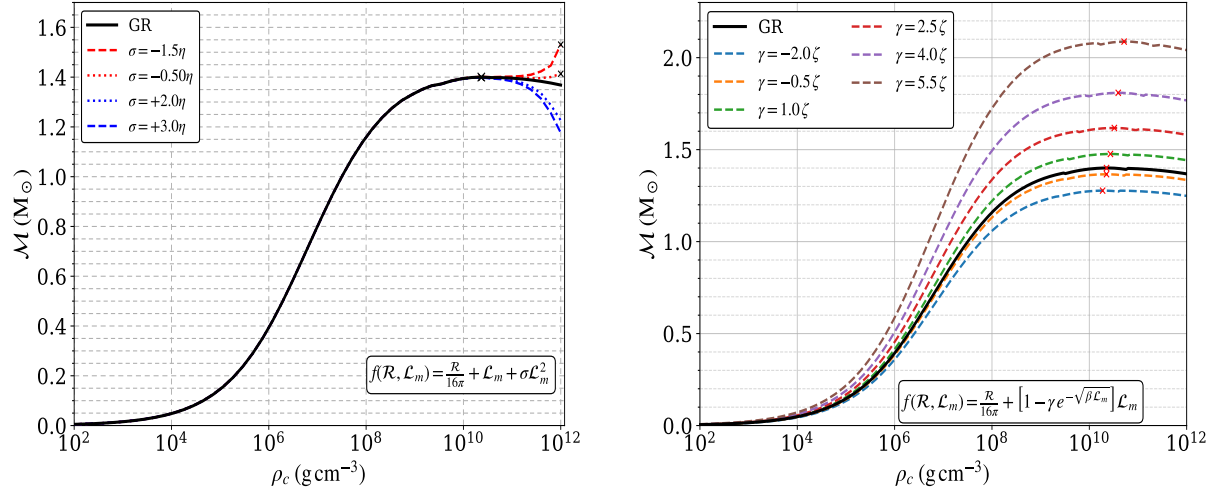


Figure 4: $M - \rho_c$ plots within the framework of the power-law and exponential models of $f(\mathcal{R}, \mathcal{L}_m)$ gravity. The solid black line represents the GR, while colored curves represent the different values of σ and γ .

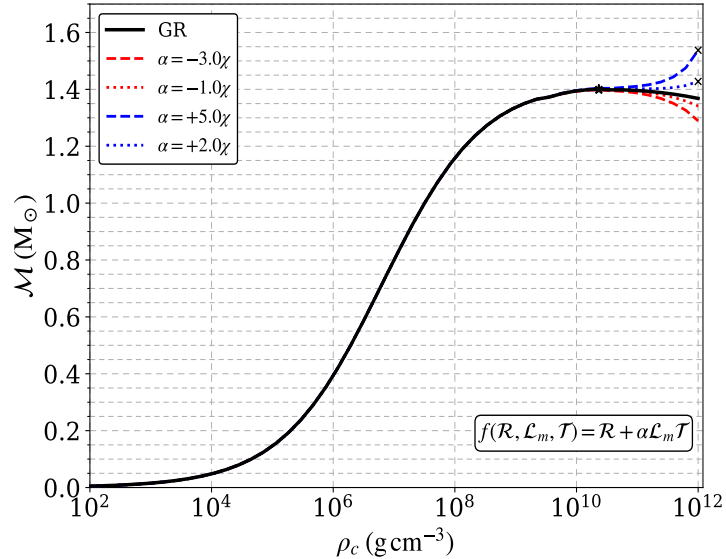


Figure 5: $M - \rho_c$ plots within the non-linear model of $f(\mathcal{R}, \mathcal{L}_m, T)$ gravity. The solid black lines represent the GR, whereas the colored curves represent the various values of the coupling parameter α .

We have analyzed $Z_s - M$ for the power-law model of the $f(\mathcal{R}, \mathcal{L}_m)$ gravity, considering both GR and parameter σ within the same ranges as previously adopted. The corresponding results are shown in the Figure 6. As expected, the very small values of compactness and redshift remained small i.e., $\mathcal{O}(10^{-3})$. Higher redshift values are obtained in the case of negative values of σ . The numerical values of compactness and

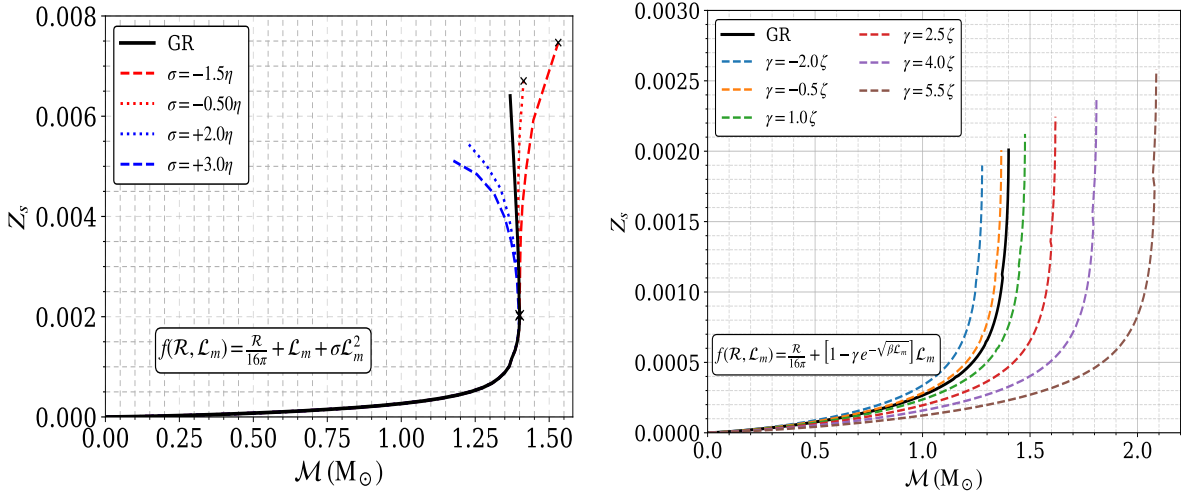


Figure 6: $Z_s - M$ plots within the framework of the power-law and exponential model models of $f(\mathcal{R}, \mathcal{L}_m)$ gravity. The solid black lines denote GR, while the colored curves illustrate different values of the coupling parameter σ and γ .

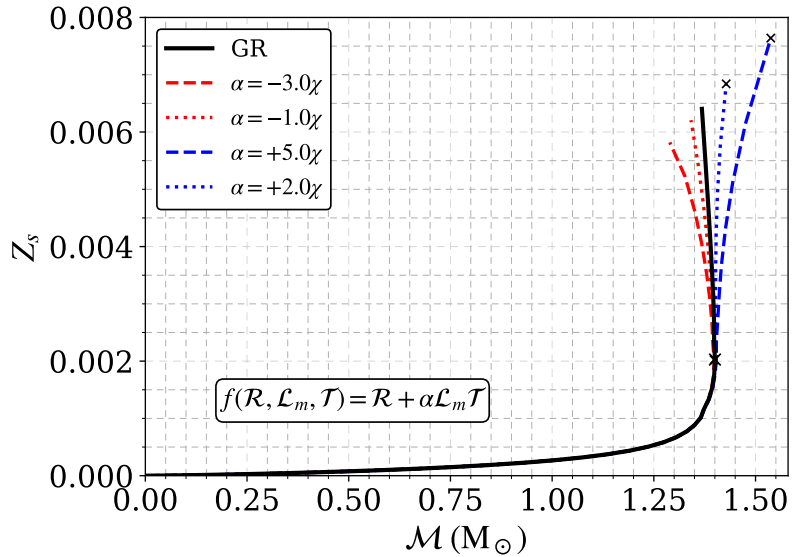


Figure 7: $Z - M$ plot for WDs within the non-linear model of $f(\mathcal{R}, \mathcal{L}_m, \mathcal{T})$ gravity. The solid black curve represents the predictions of GR, while the colored curves depict various values of the coupling parameter α .

redshift are also provided in Table 1. For the exponential model of $f(\mathcal{R}, \mathcal{L}_m)$ gravity, we have plotted the $Z_s - M$ relation for both GR and for parameter γ within the same ranges as previously considered as shown in the Figure 6. In this case, positive values of γ provided a higher redshift as compared to the GR case. We have also provided the compactness and redshift values in Table 2. Finally, we analyzed the $Z_s - M$ for the

GR and for the coupling parameter α of the non-linear model of $f(\mathcal{R}, \mathcal{L}_m, \mathcal{T})$ gravity within the same ranges. In contrast with the power-law model of $f(\mathcal{R}, \mathcal{L}_m)$ gravity, in this model, positive values of α provided the higher redshift as shown in the Figure 7. The numerical values of compactness and redshift are also provided in the Table 3.

For all the models considered, the compactness and redshift are significantly smaller than those of the NS. Due to their smaller magnitudes, the numerical values of compactness and redshift are nearly identical. Relatively higher values are obtained in power-law model of $f(\mathcal{R}, \mathcal{L}_m)$ gravity and in non-linear model of $f(\mathcal{R}, \mathcal{L}_m, \mathcal{T})$ gravity when compared to the exponential model of $f(\mathcal{R}, \mathcal{L}_m)$ gravity.

6.3 Adiabatic Index

We emphasize an important aspect of stability analysis i.e., the adiabatic index, $\Gamma(r)$. This parameter is crucial in thermodynamics, particularly under adiabatic conditions, where it defines the relationship between pressure and density. The adiabatic index illustrates how pressure changes with density during these processes. Using the variational method, Chandrasekhar [79] showed that for dynamical stability to be achieved, the condition $\Gamma > 4/3$ must be satisfied. In the relativistic regime, general relativistic corrections further enhance the onset of instability, necessitating that Γ exceeds the Newtonian limit. The relativistic formulation of the adiabatic index and its significance in stellar stability were later thoroughly discussed by Herrera et al. [80] and Misner et al. [81].

$$\Gamma = \left(\frac{\rho + p}{p} \right) \frac{dp}{d\rho}, \quad (6.2)$$

We have analyzed $\Gamma - r$ for the power-law model of the $f(\mathcal{R}, \mathcal{L}_m)$ gravity, considering both GR and parameter σ within the same ranges as previously adopted. The corresponding results are shown in the Figure 8. For both the GR and all considered values of σ , one can clearly observe that the adiabatic index $\Gamma > 4/3$, throughout the stellar interior of WDs, indicating dynamical stability. For the exponential model of $f(\mathcal{R}, \mathcal{L}_m)$ gravity, we have plotted the $\Gamma - r$ relation for both GR and for parameter γ within the same ranges as previously considered, as shown in the Figure 8. Here, the dotted line represents the value of $\Gamma = 4/3$, and all the curves lie above this limit, confirming the stability of the system. Finally, we analyzed the $\Gamma - r$ for the GR and for the coupling parameter α of the non-linear model of $f(\mathcal{R}, \mathcal{L}_m, \mathcal{T})$ gravity within the same ranges (Figure 9). The horizontal dashed line represents the critical threshold $\Gamma = 4/3$. It is evident that, for GR and for all considered values of α , the adiabatic index remains above this limit throughout the stellar interior, which satisfies the dynamical stability condition of the WDs. For all the models considered, relatively higher values are obtained in power-law model of $f(\mathcal{R}, \mathcal{L}_m)$ gravity and in non-linear model of $f(\mathcal{R}, \mathcal{L}_m, \mathcal{T})$ gravity when compared to the exponential model of $f(\mathcal{R}, \mathcal{L}_m)$ gravity. For all the models considered, the dynamical stability of the WDs is examined exclusively through the adiabatic criterion. By analyzing the adiabatic index Γ as a function of the radial coordinate, we plot the $\Gamma - r$ profile for both GR and for parameter ranges of the considered models. In all the cases, the adiabatic index remains above the critical

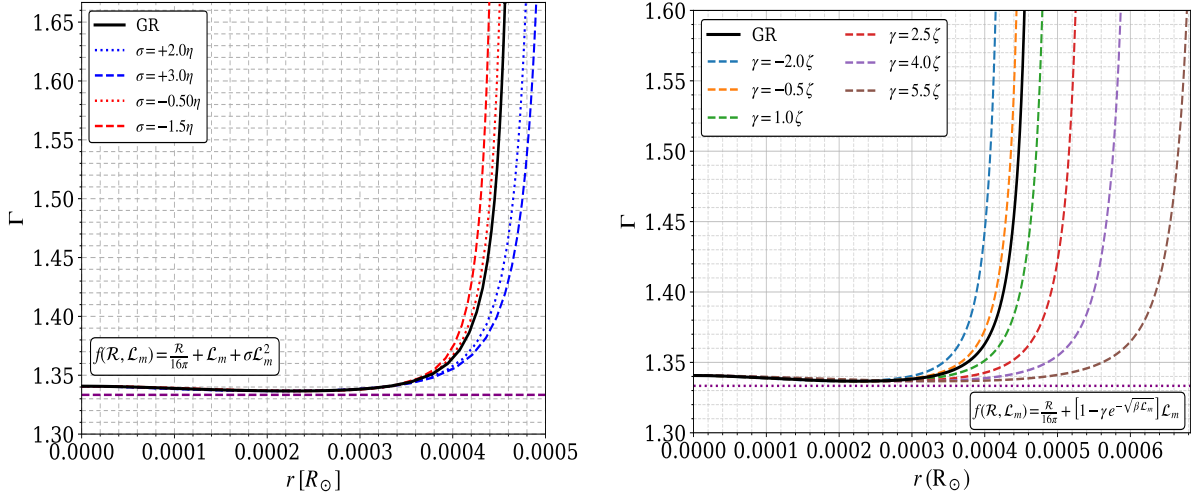


Figure 8: Adiabatic Index, Γ as a function of radial coordinate within power-law and exponential models of $f(\mathcal{R}, \mathcal{L}_m)$ gravity. The solid black line denotes the GR, while the colored lines represent the different values of σ and γ . Here, the purple dashed line represents $\Gamma = 4/3$ below which a stellar object will be unstable.

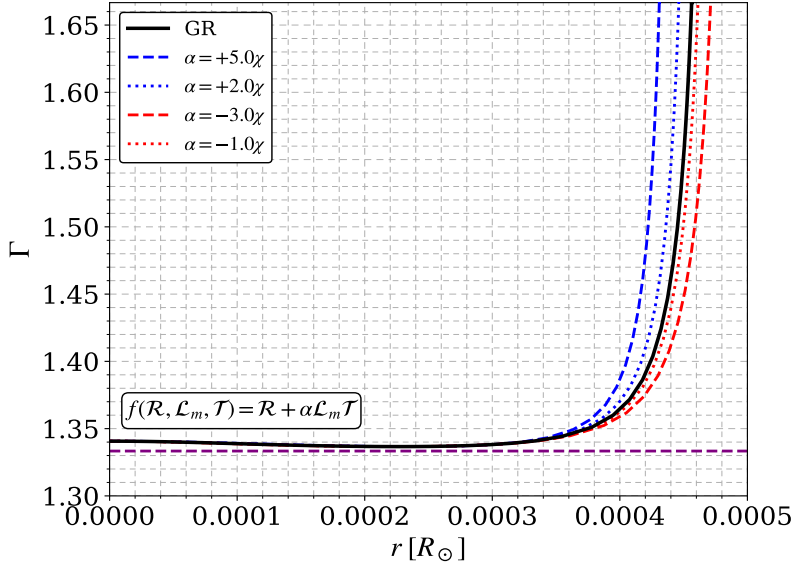


Figure 9: Adiabatic Index, Γ as a function of radial coordinate within non-linear model of $f(\mathcal{R}, \mathcal{L}_m, T)$ gravity. The solid black line denotes the GR, while the colored lines represent the different values of α . Here, the purple dashed line represents $\Gamma = 4/3$ below which a stellar object will be unstable.

value, i.e., $\Gamma > 4/3$ throughout the interior of the stellar structure, confirming the dynamical stability of the configuration.

Table 1: Structure properties of WDs configurations in $f(\mathcal{R}, \mathcal{L}_m)$ gravity: Power-law model

Parameter	\mathcal{M}_{\max} (M_\odot)	\mathcal{R}_{\max} ($R_\odot \times 10^{-3}$)	$C \times 10^{-3}$	$Z_s \times 10^{-3}$
$\sigma = -1.50\eta$	1.52	0.439	7.385	7.468
$\sigma = -0.50\eta$	1.41	0.452	6.636	6.703
$\sigma = 0$ (GR)	1.40	1.47	2.021	2.027
$\sigma = +2.0\eta$	1.39	1.47	2.019	2.025
$\sigma = +3.0\eta$	1.38	1.47	2.018	2.024

Table 2: Structure properties of WDs configurations in $f(\mathcal{R}, \mathcal{L}_m)$ gravity: Exponential model.

Parameter	\mathcal{M}_{\max} (M_\odot)	\mathcal{R}_{\max} ($R_\odot \times 10^{-3}$)	$C \times 10^{-3}$	$Z_s \times 10^{-3}$
$\gamma = -2.0\zeta$	1.27	1.43	1.893	1.898
$\gamma = -5.0\zeta$	1.36	1.45	2.001	2.007
$\gamma = 0$ (GR)	1.40	1.47	2.021	2.027
$\gamma = +1.0\zeta$	1.47	1.48	2.116	2.122
$\gamma = +2.5\zeta$	1.61	1.53	2.237	2.245
$\gamma = +4.0\zeta$	1.80	1.62	2.365	2.374
$\gamma = +5.5\zeta$	2.08	1.72	2.570	2.580

Table 3: Structure properties of WDs configurations in $f(\mathcal{R}, \mathcal{L}_m, \mathcal{T})$ gravity: Non-linear model.

Parameter	\mathcal{M}_{\max} (M_\odot)	\mathcal{R}_{\max} ($R_\odot \times 10^{-3}$)	$C \times 10^{-3}$	$Z_s \times 10^{-3}$
$\alpha = -3.0\chi$	1.398	1.471	2.017	2.023
$\alpha = -1.0\chi$	1.399	1.470	2.020	2.026
$\alpha = 0$ (GR)	1.40	1.47	2.021	2.027
$\alpha = +2.0\chi$	1.427	0.447	6.771	6.840
$\alpha = +5.0\chi$	1.537	0.432	7.553	7.639

7 Conclusions

Observations suggest that super-Chandrasekhar white dwarfs may exist, implying that the classical Chandrasekhar limit can be surpassed. This possibility has been investigated in the context of modified theories of gravity [40, 41, 46, 72, 82]. In this paper, we explore matter geometry coupled gravity, such as $f(\mathcal{R}, \mathcal{L}_m)$ and $f(\mathcal{R}, \mathcal{L}_m, \mathcal{T})$, with specific functional forms. The generalized TOV equations are solved for the functional forms of each gravity using the Chandrasekhar EoS. Further, we vary the parameters

and obtain $M - R$ relations for each functional form of $f(\mathcal{R}, \mathcal{L}_m)$ and $f(\mathcal{R}, \mathcal{L}_m, \mathcal{T})$ gravity.

For the power-law model of $f(\mathcal{R}, \mathcal{L}_m)$ gravity, the effect of the coupling parameter σ deviates from GR, and higher maximum masses are obtained for negative values of the parameter. With the values of $\sigma = -1.5\eta$ the model provide $1.5M_\odot$ with radius about $0.439 \times 10^{-3} R_\odot$ (Figure 1). Similar results are observed in the non-linear form of $f(\mathcal{R}, \mathcal{L}_m, \mathcal{T})$ gravity. With $\alpha\mathcal{R}\mathcal{T}$ coupling term, the maximum mass exceeds the Chandrasekhar limit and increases with the increase of α . For $\alpha = +5.0\chi$, $f(\mathcal{R}, \mathcal{L}_m, \mathcal{T})$ gravity with non-linear case provided the maximum mass of $1.537 M_\odot$ and radius of $0.432 \times 10^{-3} R_\odot$ (Figure 3). Finally, we consider the exponential model in the framework of the $f(\mathcal{R}, \mathcal{L}_m)$ gravity. In this form, the deviation in masses is clearly observed and the maximum mass exceeds the Chandrasekhar limit and increases with increasing γ . For $\gamma = +5.5\zeta$, the model obtain maximum mass up to $2.08 M_\odot$ with the radius of $1.72 \times 10^{-3} R_\odot$ (Figure 2). To assess physical viability, we analyzed WDs stability using several criteria. We have analyzed the static stability criterion where $dM/d\rho_c > 0$. All the functional forms of each gravity show an increase in mass with increasing central density up to the a maximum mass, which satisfies the stability condition (Figures 4 and 5). Also, we analyze compactness and gravitational redshift and find that, in each model of $f(\mathcal{R}, \mathcal{L}_m)$ and $f(\mathcal{R}, \mathcal{L}_m, \mathcal{T})$ gravity, the values are of order $\mathcal{O}(10^{-3})$, which is very small compared to those of NSs and BHs. Finally, we have confirmed that WDs of each the functional forms of $f(\mathcal{R}, \mathcal{L}_m)$ and $f(\mathcal{R}, \mathcal{L}_m, \mathcal{T})$ gravity are dynamically stable by analyzing the adiabatic index. For each model, the adiabatic indices remain above the critical value i.e., $\Gamma > 4/3$ throughout the interior of the WDs (Figures 8 and 9).

Overall, our results indicate that there might be a super-Chandrasekhar WDs maximum mass limit that differs from the existing limit in the Newtonian scenario. Further, one can analyze with strong magnetic fields, i.e., coupled with the Maxwell equations, and also consider a multi-component thermal EoS composed of He-C-O to examine the effects on the structure properties.

Acknowledgement

NP acknowledges the financial support provided by the University Grants Commission (UGC) through the Junior Research Fellowship (UGC Ref. No.: 231620138510) to carry out the research work. KNS and BM acknowledge the support of IUCAA, Pune (India), through the visiting associateship program. The SKM is also grateful to the UoN administration for its continued support and encouragement of the research work.

References

- [1] A. Einstein, *Erklärung der Perihelbewegung des Merkur aus der allgemeinen Relativitätstheorie, Sitzungsber. Kgl. Preuss. Akad. Wiss.* (1915) 831.
- [2] B.P. Abbott and et al., *Observation of Gravitational Waves from a Binary Black Hole Merger, Phys. Rev. Lett.* **116** (2016) 061102.
- [3] B.P. Abbott, R. Abbott, T.D. Abbott et al., *GW170817: Observation of Gravitational Waves from a Binary Neutron Star Inspiral, Phys. Rev. Lett.* **119** (2017) 161101.
- [4] K. Akiyama, A. Alberdi et al., *First M87 Event Horizon Telescope Results. I. The Shadow of the Supermassive Black Hole, Astrophys. J. Lett.* **875** (2019) L1.
- [5] A.G. Riess, A.V. Filippenko, P. Challis et al., *Observational Evidence from Supernovae for an Accelerating Universe and a Cosmological Constant, Astrophys. J.* **116** (1998) 1009.
- [6] Perlmutter, S. and Aldering, G. and Goldhaber, G. and others, *Measurements of Ω and Λ from 42 High-Redshift Supernovae, Astrophys. J.* **517** (1999) 565.
- [7] R.A. Knop, G. Aldering, R. Amanullah et al., *New Constraints on Ω_M , Ω_Λ , and w from an Independent Set of 11 High-Redshift Supernovae Observed with the Hubble Space Telescope, Astrophys. J.* **598** (2003) 102.
- [8] R. Amanullah, C. Lidman, D. Rubin et al., *Spectra and Hubble Space Telescope Light Curves of Six Type Ia Supernovae at $0.511 < z < 1.12$ and the Union2 Compilation*, Astrophys. J.* **716** (2010) 712.
- [9] D.H. Weinberg, M.J. Mortonson, D.J. Eisenstein et al., *Observational probes of cosmic acceleration, Phys. Rep.* **530** (2013) 87.
- [10] S.L. Shapiro and S.A. Teukolsky, *Black holes, white dwarfs, and neutron stars: The physics of compact objects* (1983), [10.1002/9783527617661](https://doi.org/10.1002/9783527617661).
- [11] G.R. Lauffer, A.D. Romero and S.O. Kepler, *New full evolutionary sequences of H- and He-atmosphere massive white dwarf stars using mesa, Mon. Not. R. Astron. Soc.* **480** (2018) 1547.
- [12] S.E. Woosley and A. Heger, *The Remarkable Deaths of 9-11 Solar Mass Stars, Astrophys. J.* **810** (2015) 34.
- [13] S. Chandrasekhar, *The Maximum Mass of Ideal White Dwarfs, Astrophys. J.* **74** (1931) 81.
- [14] S. Chandrasekhar, *The highly collapsed configurations of a stellar mass, Mon. Not. R. Astron. Soc.* **91** (1931) 456.
- [15] D. Andrew Howell, M. Sullivan, P.E. Nugent et al., *The type Ia supernova SNLS-03D3bb from a super-Chandrasekhar-mass white dwarf star, Nature* **443** (2006) 308.
- [16] R. Scalzo, G. Aldering, P. Antilogus, C. Aragon et al., *Nearby supernova factory observations of SN 2007if: First total mass measurement of a super-Chandrasekhar-mass progenitor, Astrophys. J.* **713** (2010) 1073.

- [17] M. Yamanaka, K.S. Kawabata, K. Kinugasa et al., *Early phase observations of extremely luminous Type Ia Supernova 2009dc*, *Astrophys. J.* **707** (2009) L118.
- [18] J.M. Silverman, M. Ganeshalingam and A.V. Filippenko, *Berkeley Supernova Ia Program – V. Late-time spectra of Type Ia Supernovae*, *Mon. Not. R. Astron. Soc.* **430** (2013) 1030.
- [19] A.V. Filippenko, M.W. Richmond, D. Branch et al., *The subluminous, spectroscopically peculiar Type Ia supernova 1991bg in the elliptical galaxy NGC 4374*, *Astron. J.* **104** (1992) 1543.
- [20] S. Taubenberger, S. Hachinger, G. Pignata, P.A. Mazzali et al., *The underluminous Type Ia supernova 2005bl and the class of objects similar to SN 1991bg**, *Mon. Not. R. Astron. Soc.* **385** (2008) 75.
- [21] M. Turatto, A. Piemonte, S. Benetti et al., *A New Faint Type Ia Supernova: SN 1997cn in NGC 5490*, *Astron. J.* **116** (1998) 2431–2437.
- [22] M. Hicken, P.M. Garnavich, J.L. Prieto et al., *The Luminous and Carbon-rich Supernova 2006gz: A Double Degenerate Merger?*, *Astrophys. J.* **669** (2007) L17.
- [23] A. Khokhlov, E. Müller and P. Höflich, *Light curves of type IA supernova models with different explosion mechanisms*, *Astron. & Astrophys.* **270** (1993) 223.
- [24] H.A. Buchdahl, *Non-linear Lagrangians and cosmological theory*, *Mon. Not. R. Astron. Soc.* **150** (1970) 1.
- [25] S. Capozziello and M. De Laurentis, *Extended Theories of Gravity*, *Phys. Rep.* **509** (2011) 167.
- [26] A. De Felice and S. Tsujikawa, *$f(R)$ Theories*, *Living Rev. Relativ.* **13** (2010) .
- [27] S. Capozziello, S. Nojiri, S. Odintsov et al., *Cosmological viability of $f(R)$ gravity as an ideal fluid and its compatibility with a matter dominated phase*, *Phys. Lett. B* **639** (2006) 135.
- [28] L. Amendola and S. Tsujikawa, *Phantom crossing, equation-of-state singularities, and local gravity constraints in $f(R)$ models*, *Phys. Lett. B* **660** (2008) 125.
- [29] S. Tsujikawa, *Observational signatures of $f(R)$ dark energy models that satisfy cosmological and local gravity constraints*, *Phys. Rev. D* **77** (2008) 023507.
- [30] T. Liu, X. Zhang and W. Zhao, *Constraining $f(R)$ gravity in solar system, cosmology and binary pulsar systems*, *Phys. Lett. B* **777** (2018) 286.
- [31] A.V. Astashenok, S. Capozziello and S.D. Odintsov, *Further stable neutron star models from $f(R)$ gravity*, *J. Cosmol. Astropart. Phys.* **2013** (2013) 040.
- [32] Nashed, Gamal G. L. and Odintsov, Sergei D. and Oikonomou, Vasillis K., *Anisotropic Compact Stars in $D \rightarrow 4$ Limit of Gauss–Bonnet Gravity*, *Symmetry* **14** (2022) 545.
- [33] G.G.L. Nashed and S. Capozziello, *Anisotropic compact stars in $f(R)$ gravity*, *Eur. Phys. J. C* **81** (2021) 481.
- [34] A.V. Astashenok, S. Capozziello et al., *Extended Gravity Description for the GW190814 Supermassive Neutron Star*, *Phys. Lett. B* **811** (2020) 135910.
- [35] S. Capozziello, M. De Laurentis et al., *Mass-radius relation for neutron stars in $f(R)$ gravity*, *Phys. Rev. D* **93** (2016) 023501.

[36] A. Astashenok, S. Capozziello, S. Odintsov et al., *Causal limit of neutron star maximum mass in $f(R)$ gravity in view of GW190814*, *Physics Letters B* **816** (2021) 136222.

[37] A. Ganguly, R. Gannouji, R. Goswami et al., *Neutron stars in the Starobinsky model*, *Phys. Rev. D* **89** (2014) 064019.

[38] A.V. Astashenok, S.D. Odintsov and S. de la Cruz-Dombriz, *The realistic models of relativistic stars in $f(R) = R + \alpha R^2$ gravity*, *Class. Quant. Grav.* **34** (2017) 205008.

[39] A.V. Astashenok, S. Capozziello and S.D. Odintsov, *Extreme neutron stars from Extended Theories of Gravity*, *J. Cosmol. Astropart. Phys.* **2015** (2015) 001.

[40] U. Das and B. Mukhopadhyay, *Modified Einstein's gravity as a possible missing link between sub-and super-Chandrasekhar type Ia supernovae*, *J. Cosmol. Astropart. Phys.* **2015** (2015) 045.

[41] S. Banerjee, S. Shankar and T.P. Singh, *Constraints on modified gravity models from white dwarfs*, *J. Cosmol. Astropart. Phys.* **2017** (2017) 004.

[42] S. Kalita and B. Mukhopadhyay, *Modified Einstein's gravity to probe the sub-and super-Chandrasekhar limiting mass white dwarfs: a new perspective to unify under-and over-luminous type Ia supernovae*, *J. Cosmol. Astropart. Phys.* **2018** (2018) 007.

[43] R.K. Jain, C. Kouvaris and N.G. Nielsen, *White Dwarf Critical Tests for Modified Gravity*, *Phys. Rev. Lett.* **116** (2016) 151103.

[44] A.V. Astashenok, S.D. Odintsov and V.K. Oikonomou, *Maximal masses of white dwarfs for polytropes in R^2 gravity and theoretical constraints*, *Phys. Rev. D* **106** (2022) 124010.

[45] G.A. Carvalho, R.V. Lobato, P.H.R.S. Moraes et al., *Stellar equilibrium configurations of white dwarfs in the $f(R, T)$ gravity*, *Eur. Phys. J. C* **77** (2017) 871.

[46] F. Rocha, G. Carvalho, D. Deb and M. Malheiro, *Study of the charged super-Chandrasekhar limiting mass white dwarfs in the $f(R, T)$ gravity*, *Phys. Rev. D* **101** (2020) 104008.

[47] S. Kalita and L. Sarmah, *Weak-field limit of $f(R)$ gravity to unify peculiar white dwarfs*, *Phys. Lett. B* **827** (2022) 136942.

[48] S. Kalita, L. Sarmah and A. Wojnar, *Metric-affine effects in crystallization processes of white dwarfs*, *Phys. Rev. D* **107** (2023) 044072.

[49] Li, Jie and Yang, Bo and Lin, Wenbin, *Massive white dwarfs in Rastall-Rainbow gravity*, *J. Cosmol. Astropart. Phys.* **04** (2024) 081.

[50] S. Vidal, A. Wojnar, L. Järv et al., *Crystallized white dwarf stars in scalar-tensor gravity*, *Phys. Rev. D* **111** (2025) 084075.

[51] O. Bertolami and M.C. Sequeira, *Energy conditions and stability in $f(R)$ theories of gravity with nonminimal coupling to matter*, *Phys. Rev. D* **79** (2009) 104010.

[52] T. Harko, *The matter Lagrangian and the energy-momentum tensor in modified gravity with nonminimal coupling between matter and geometry*, *Phys. Rev. D* **81** (2010) 044021.

[53] F.S.N. Lobo, T. Harko and M.A.S. Pinto, *Modified gravity with nonminimal curvature-matter couplings: A framework for gravitationally induced particle creation*, *Universe* **11** (2025) 356.

[54] T. Harko and F.S.N. Lobo, *$f(R, L_m)$ gravity*, *Eur. Phys. J. C* **70** (2010) 373.

[55] V. Faraoni, *Lagrangian description of perfect fluids and modified gravity with an extra force*, *Phys. Rev. D* **80** (2009) 124040.

[56] O. Bertolami, J. Paramos and S.G. Turyshev, *General theory of relativity: Will it survive the next decade?*, *Astrophys. Space Sci. Libr.* **349** (2008) 27.

[57] R. Lobato, G. Carvalho, N. Kelkar et al., *Massive white dwarfs in $f(R, L_m)$ gravity*, *Eur. Phys. J. C* **82** (2022) 540.

[58] R.V. Lobato, G.A. Carvalho and C.A. Bertulani, *Neutron stars in $f(R, L_m)$ gravity with realistic equations of state: joint-constraints with GW170817, massive pulsars, and the PSR J0030+0451 mass-radius from NICER data*, *Eur. Phys. J. C* **81** (2021) 1013.

[59] F.S.N. Lobo and M.A. Oliveira, *Wormhole geometries in $f(R)$ modified theories of gravity*, *Phys. Rev. D* **80** (2009) 104012.

[60] A.S. Agrawal, B.K. Lotte, R. Kapse et al., *Exploring Wormhole Structures within the Framework of $f(R, L_m)$ Gravity*, [2509.17497](#).

[61] M. Khatri and J. Lalvohbika, *Casimir wormhole solutions in $f(R, L_m)$ gravity*, *Chin. J. Phys.* **89** (2024) 1222.

[62] J. Wang and K. Liao, *Energy conditions in $f(R, L_m)$ gravity*, *Class. Quantum Grav.* **29** (2012) 215016.

[63] S. Nesseris, *Matter density perturbations in modified gravity models with arbitrary coupling between matter and geometry*, *Phys. Rev. D* **79** (2009) 044015.

[64] B. Gonçalves, P. Moraes and B. Mishra, *Cosmology from Non-Minimal Geometry-Matter Coupling*, *Fortsch. Phys.* **71** (2023) 2200153.

[65] T. Harko, *Galactic rotation curves in modified gravity with nonminimal coupling between matter and geometry*, *Phys. Rev. D* **81** (2010) 084050.

[66] T. Harko, F.S.N. Lobo, S. Nojiri et al., *$f(R, T)$ gravity*, *Phys. Rev. D* **84** (2011) 024020.

[67] Z. Haghani and T. Harko, *Generalizing the coupling between geometry and matter: $f(R, L_m, T)$ gravity*, *Eur. Phys. J. C* **81** (2021) 615.

[68] N. Priyobarta, K.N. Singh, S. Maurya et al., *Realistic modeling of neutron star structures with linear and non-linear matter-curvature coupling in $f(R, L_m, T)$ -gravity using SLy4, Togashi, and Walecka equation of state*, *Chin. J. Phys.* **99** (2026) 162.

[69] P. Moraes, A. Agrawal and B. Mishra, *Wormholes in the $f(R, L, T)$ theory of gravity*, *Phys. Lett. B* **855** (2024) 138818.

[70] C.E. Mota, J.M.Z. Pretel and C.O.V. Flores, *Neutron stars in $f(R, L_m, T)$ gravity*, *Eur. Phys. J. C* **84** (2024) 673.

[71] V. A. Kshirsagar and A. S. Agrawal and S. A. Kadam and others, *Cosmological Dynamics in $f(R, L_m, T)$ Modified Gravity*, [2511.14309](#).

[72] E. Otoniel, J.M.Z. Pretel, C.E. Mota et al., *White dwarf structure in $f(R, T, L_m)$ gravity: beyond the Chandrasekhar mass limit*, [2507.18745](#).

[73] Landau, L. D. and Lifschits, E. M., *The Classical Theory of Fields*, vol. Volume 2 of *Course of Theoretical Physics*, Pergamon Press, Oxford (1975).

[74] T. Koivisto, *Covariant conservation of energy momentum in modified gravities*, *Class. Quant. Grav.* **23** (2006) 4289.

[75] N. Priyobarta, K.N. Singh, S.K. Maurya et al., *Constraining radii and stability of neutron stars in 4D Einstein–Gauss–Bonnet gravity*, *Chin. J. Phys.* **96** (2025) 1164.

[76] A. Bédard, P. Bergeron and G. Fontaine, *Measurements of Physical Parameters of White Dwarfs: A Test of the Mass–Radius Relation*, *Astrophys. J.* **848** (2017) 11.

[77] I. Caiazzo, K.B. Burdge, J. Fullear et al., *A highly magnetized and rapidly rotating white dwarf as small as the Moon*, *Nature* **595** (2021) 39–42.

[78] M.A. Barstow, S. Jordan, D. O’Donoghue et al., *Re j0317 – 853: the hottest known highly magnetic da white dwarf*, *Mon. Not. R. Astron. Soc.* **277** (1995) 971.

[79] S. Chandrasekhar, *Dynamical instability of gaseous masses approaching the Schwarzschild limit in general relativity*, *Astrophys. J.* **140** (1964) 417C.

[80] L. Herrera, G. Le Denmat and N. Santos, *Dynamical instability for non-adiabatic spherical collapse*, *Mon. Not. R. Astron. Soc.* **237** (1989) 257.

[81] C.W. Misner, K.S. Thorne and J.A. Wheeler, *Gravitation*, W. H. Freeman (1973).

[82] J. Li, B. Yang and W. Lin, *Color-flavor locked quark stars in Rastall-Rainbow gravity*, *Chin. J. Phys.* **89** (2024) 134.